

Laser-Induced Graphitisation of Diamond Under 30 fs Laser Pulse Irradiation

AUTHORS

Bakhtiar Ali ^{a, b}, Han Xu ^{b, c}, Dashavir Chetty ^{b, c}, Robert T. Sang ^{b, c}, Igor V. Litvinyuk ^{b, c},
Maksym Rybachuk ^{a, b*}

AFFILIATIONS

^a School of Engineering and Built Environment, Griffith University, 170 Kessels Rd.,
Nathan QLD 4111, AUSTRALIA

^b Centre for Quantum Dynamics and Australian Attosecond Science Facility, Griffith
University, Science Road, Nathan, QLD, 4111, AUSTRALIA

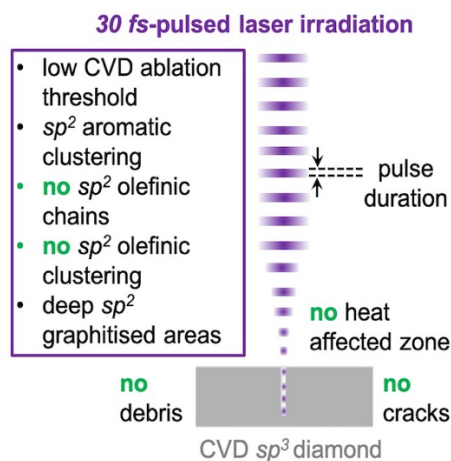
^c School of Environment and Science, Griffith University, Nathan QLD 4111,
AUSTRALIA

* Corresponding author:

m.rybachuk@griffith.edu.au

<https://orcid.org/0000-0002-5313-9204>

TOC Graphic



ABSTRACT

The degree of laser-induced graphitisation from a sp^3 -bonded to a sp^2 -bonded carbon fraction in a single crystal chemical vapour deposited (CVD) diamond under a varying fluence of an ultrashort pulsed laser (30 fs, 800 nm, 1 kHz) irradiation has been studied. The tetrahedral CVD sp^3 -phase was found to transition to primarily an sp^2 -aromatic crystalline graphitic fraction below the critical fluence of 3.9 J/cm², above which predominantly an amorphous carbon was formed. A fractional increase of fluence from 3.3 J/cm² to 3.9 J/cm² (~ 20 %) resulted in a substantial (~ three-fold) increased depth of the sp^2 -graphitised areas owing to the non-linear interactions associated with an fs-laser irradiation. Additionally, formation of C=O carbonyl group was observed below the critical threshold fluence; the C=O cleavage occurred gradually with the increase of irradiation fluence of 30 fs laser light. The implications for these findings on enhancement of fs-driven processing of diamond are discussed.

KEYWORDS

Diamond; graphite; femtosecond laser irradiation; phase change; photoionization

Highly localised and geometrically confined structural transformations in diamond with intrinsic sp^3 diamond's tetrahedral phase converted into sp^2 -rich graphitic fraction employing a laser light have shown to significantly enhance light absorption in the irradiated areas and, to open a new avenue for the emerging opto-phonic applications, including miniaturised thermionic solar cells¹, broad-beam light detectors²⁻³ and most recently, robust broad-beam polarization filters for infra-red (IR) applications⁴. These applications, however, may only become technologically accomplishable once the thermal stresses associated with laser processing and the formation of sp^2 fraction on the surface or in the bulk of the diamond crystal, are minimised while remaining spatially confined. Additionally, owing to a close lattice match between the diamond's sp^3 tetrahedral fraction and the planar two-dimensional (2D) graphene and graphite structures, direct fabrication of 'graphene-on-diamond' heterostructures by means of an *in situ* sp^3 -to- sp^2 conversion enables a development of a variety of robust ultra-wide bandgap 'all carbon' opto-electronic devices in a single-step fabrication process, without resorting to processes that normally require high-temperature annealing with a metal catalyst.⁵⁻

6

Conventional nano- (*ns*-) and pico- (*ps*-) second pulsed lasers transform diamond into graphite by means of a localised phonon-induced graphitization and, owing to their long laser-lattice interactions, primarily an amorphous sp^2 phase is formed in the heat affected zone (HAZ) marked by the appearance of thermally-induced cracks.⁷ The ultrashort femtosecond (*fs*) laser pulses generate minimal to no HAZ and produce no HAZ-associated localised cracking as the *fs* pulse ends before the excited electrons are able to transfer their energy to the diamond lattice as the characteristic time of electron-lattice interaction is a few *ps*, at least an order of magnitude longer than the pulse duration.⁸⁻⁹ However, it is known that pulses as short as 100 *fs* still thermalise electrons and generate hot ions and phonons leading to thermal quenching and sp^3 lattice relaxation in diamond.^{7, 10-12} It has been postulated that pulses shorter than 50 *fs* display

primarily non-thermal characteristics as photo-ablation and structural re-organisation is predominantly driven by photo-ionization of electrons.^{10, 13} The sub-50 fs regime still remains largely unexplored for processing of diamond.⁷ The volumetric processing efficiency, that is the sp^3 into sp^2 phase conversion, followed by a subtractive sp^2 fraction removal, remains low for all pulse widths and the lengths of the laser pulse being used, as the thermal diffusion is primarily limited to the focal volume.¹⁴ Processing diamond above its graphitisation threshold with ns - and/or ps - pulses is associated with a higher volume/mass removal but also with a significant and unavoidable formation of HAZ as longer pulses generate plasma plumes of higher ion density and electron temperature.^{9, 15} fs -pulses and, in particular, the sub-50 fs pulses are able to deliver a fluence well above the diamond's graphitization threshold (0.3 J/cm^2)¹⁶ at or near the ablation threshold ($\sim 3.0 - 4.0 \text{ J/cm}^2$)¹⁷⁻¹⁸ and, notionally, without any thermal damage. Simulations suggest that under ns - or longer laser pulse durations, graphitization propagates vertically affecting the bulk of the focal volume, leading to the formation of largely amorphous (a -) $sp^3:sp^2$ interfaces following the laser treatment¹⁹⁻²⁰. By contrast, with fs - laser pulses, graphitization of diamond occurs fully layer by layer in a *pseudo* 'peel off' process, resulting in the formation of a clean diamond surface after the ablation that is highly desirable for applied applications.

In this work, we present a preliminary experimental study on graphitisation of diamond employing an ultra-short laser pulse duration and demonstrate that a 30 fs photo-ablation of a single crystal CVD below its critical ablation threshold results primarily in a formation of sp^2 -aromatic graphitic fraction with a minimal amorphization, and in an instance when the fluence near or at the ablation threshold is used, a substantial increase (\sim three-fold) of the formed sp^2 -graphitised layer on the CVD is observed. Fractional formation of C=O carbonyl group was also observed within the sp^2 graphitised regions under all irradiation condition. Our findings demonstrate a potential for the successful use of ultra-short duration laser pulses for processing

of CVD and its derivatives (*i.e.*, natural diamond, nano- and micro-diamonds, bucky-diamond particles) for fabrication of diamond systems with previously unattainable composition and properties and, *fs* laser-assisted plating and sintering applications.

An 800 nm Ti³⁺:sapphire laser system (FEMTOPOWER™ compact™ PRO HE, FEMTOLASERS Produktions GmbH, Austria) delivering a linearly polarized Gaussian beam with a 30 *fs* pulse duration at 1 kHz repetition rate was used to irradiate an *n*-type <100> Ib CVD diamond samples (3×3×1 mm) with ~200 ppm of nitrogen content (Chenguang Machinery & Electric Equipment Co. Ltd., Hunan, China). The source pulse energy of 0.8 mJ was attenuated to 5.4 μJ, 3.1 μJ, 2.6 μJ and 1.7 μJ using pellicle beam splitters producing a laser peak fluence of 6.8 J/cm², 3.9 J/cm², 3.3 J/cm² and 2.2 J/cm² and, a peak intensity of 2.3 ×10¹⁴ W/cm², 1.3 ×10¹⁴ W/cm², 1.1 ×10¹⁴ W/cm² and 0.73 ×10¹⁴ W/cm², respectively. An 90° off-axis parabolic silver mirror and a CMOS camera beam profiler (BC207VIS(/M), Thorlabs Inc., USA) with Beam™ software package were used to precisely focus the *fs*-laser beam over the CVD diamond sample surface. The focal spot size of the beam was 10 μm at 1/e of the maximum intensity with an M² of 1.3 for all experiments. The samples positioned normal to the beam were irradiated at a scanning speed of 15 mm/s, 667 pulses per irradiation site. No self-phase modulation and/or filamentation in front of the focal point has been observed during the experiments. Unpolarised 514 nm Ar⁺ ion laser (Renishaw inVia™, UK) was used to obtain micro-Raman spectra at 293 K from the laser-irradiated samples at 1 cm⁻¹ resolution and using 0.1 mW power over an extended acquisition time to minimise possible thermal damage to CVD samples. Fully symmetric Gaussians were used to re-constitute Raman bands following a linear photoluminescence (PL) background subtraction employing a non-linear least squares fitting procedure²¹; the coefficients of determination, R², of >0.99 were obtained for all fits. Sample surface topography was studied using optical (NIKON Eclipse E-200, Japan) and scanning electron microscopy (SEM) (JSM-6510, JEOL Ltd., Japan).

Figure 1(a) displays Raman spectra obtained from laser-induced graphitized tracks *ca.* 10 μm wide on CVD at varying fluence, including the sp^3 tetrahedral diamond mode at $\sim 1332\text{ cm}^{-1}$ corresponding to the triply degenerate optical phonon of core T_{2g} symmetry near the centre of the Brillouin zone with a sharp line with the half width at half maximum (HWHM) of $\sim 6\text{ cm}^{-1}$, the core sp^2 D and G modes at *ca.* 1350 cm^{-1} and *ca.* 1582 cm^{-1} corresponding to Raman active A_{1g} and E_{2g} modes, respectively, and a carbonyl group ($-\text{C}=\text{O}$) mode at *ca.* 1710 cm^{-1} .²²⁻²⁵ The spectra display a pronounced PL scattering background associated with hydrogenation.²⁶⁻²⁹ The PL gradient increased with increasing fluence, whereas the $\sim 1332\text{ cm}^{-1}$ diamond mode gradually receded and almost completely resolved at 6.8 J/cm^2 (blue spectrum), indicating significant graphitisation of irradiated areas on CVD.³⁰

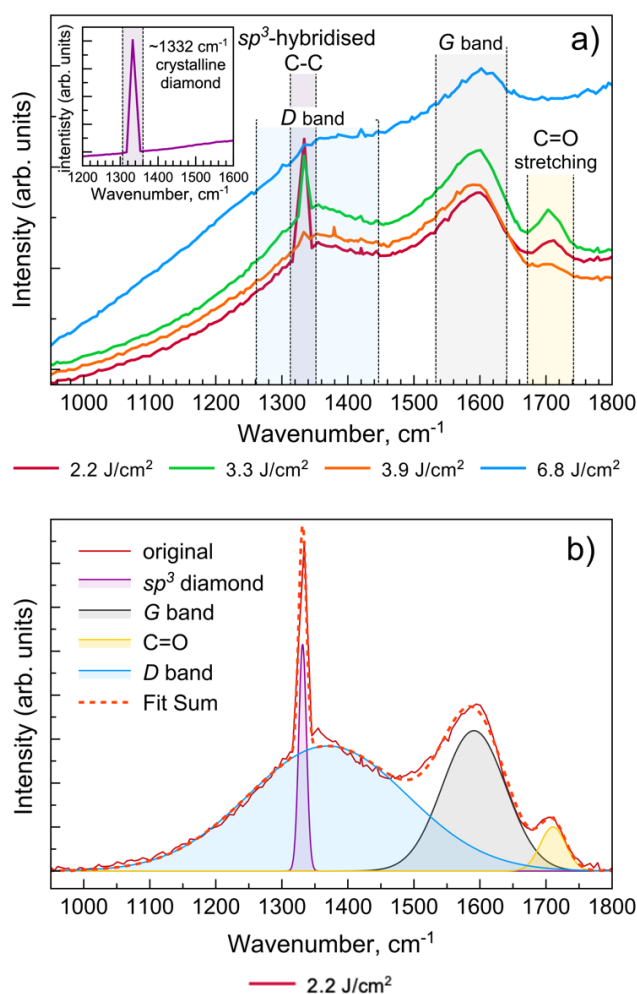


Fig. 1a) 514 nm Raman spectra of 30 fs-laser irradiated CVD at varying fluence, b) example of a deconvoluted Raman spectra of CVD irradiated at 2.2 J/cm² fluence showing the constituent *sp*³ (1332 cm⁻¹) diamond band, and *D*, *G* and C=O bands.

Fig. 1b) shows deconvoluted Raman spectra of CVD irradiated at 2.2 J/cm² fluence. The constituent *sp*³ tetrahedral diamond mode at ~1332 cm⁻¹, and *D*, *G* and C=O bands are clearly visible. Detailed analysis of Raman spectra, as shown in Fig. 2a-c, revealed two distinct spectral characteristics of fs-pulsed laser irradiated CVD samples as shown by the evolution of relative ratios of the *D* to the *G* peak, $I(D)/I(G)$ (Fig. 2a), their respective HWHM values (Fig. 2b) and, relative positions of the *D*, *D_r* and the *G*, *G_r* peaks (Fig. 2c) at increasing fluence. Notably, the $I(D)/I(G)$ ratio increased from 0.89 to 1.05, whereas the effective crystallite size, L_a , measured in nm, which was initially defined by Tuinstra and Koenig²⁷ and given by Cançado *et. al.*³¹ for 514 nm laser excitation, E (*i.e.*, 2.41 eV), using the Eq. (1)

$$L_a = \frac{560}{E^4} \left(\frac{I(D)}{I(G)} \right)^{-1}, \quad (1)$$

was found to decrease from approximately 19 nm to 16 nm at increasing fluence from 2.2 J/cm² to 3.9 J/cm² (see Fig. 2a), indicating increasing *sp*² aromatic clustering near the K and M points of the Brillouin zone and corresponding the overall reduction of crystallinity.^{23,32}

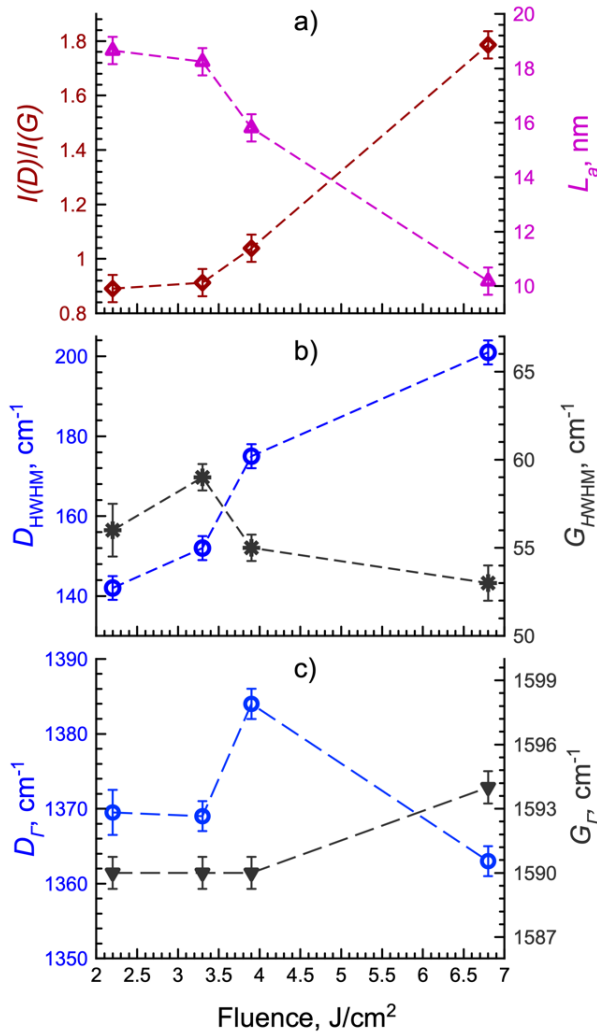


Fig. 2. Characteristic features of Raman spectra of 30 fs-laser irradiated CVD, including a) $I(D)/I(G)$ peak ratios and effective crystallite size, L_a , b) HWHM values for the D and the G peaks and, c) positions of the D and G peaks at varying fluence.

These observations are commensurate with those reported by Girolami *et. al.*³² for 100-fs irradiation for fluences that are far below the ablation threshold for diamond. The latter, evidently, provide insufficient energy to convert significant volume/mass of diamond to graphite to attain any practical sample processing efficiency. As the fluence increases to 6.8 J/cm² the $I(D)/I(G)$ ratio almost doubles to *ca.* 1.6, whereas the L_a is reduced by ~50% (Fig. 2a) down to 10 nm, which corresponds to a further increase of sp^2 aromatic clustering, and the

reduction of sp^2 crystallinity in the 30 fs-irradiated regions of CVD samples.²³⁻²⁴ Likewise, the D_{HWHM} (Fig. 2b) increases from *ca.* 140 cm^{-1} to *ca.* 175 cm^{-1} with increasing fluence from 2.2 J/cm^2 to 3.9 J/cm^2 indicating an increase of structural disorder of sp^2 aromatic clusters^{23, 33-34}, followed by a unambiguous increase to over *ca.* 200 cm^{-1} as the fluence is increased to 6.8 J/cm^2 , confirming significant sp^2 amorphization²⁵ in the 30 fs-irradiated regions^{27, 35}.

High quality of sp^3 converted graphite-like clustering is observed up to 3.9 J/cm^2 , except for the highest applied fluence of 6.8 J/cm^2 , for which the D_{HWHM} is sharply increased, indicating an increase in amorphization²⁵. The G_{HWHM} (Fig. 2b) values remain largely unchanged indicating that the sp^2 fractional disorder is marginally affected by the increasing fluence above the diamond ablation threshold. The D peak redshifts about 15 cm^{-1} (Fig. 2c) as the fluence is increased from 2.2 J/cm^2 to 3.9 J/cm^2 , corresponding to the increase of sp^2 aromaticity³⁵ and, as the fluence is further increased to 6.8 J/cm^2 the D peak blueshifts *ca.* 20 cm^{-1} (Fig. 3c) as an indication of increasing amorphization of the sp^2 fraction, in accordance with the earlier observations for $I(D)/I(G)$ ratio and the D_{HWHM} and the G_{HWHM} changes. The G_r slightly blueshifts from 1590 cm^{-1} to 1594 cm^{-1} as the fluence is increased from 2.2 J/cm^2 to 6.8 J/cm^2 . The G_r position below 1600 cm^{-1} as noted by Ferrari *et al.*³⁶ is attributed to an exclusive presence of aromatic rings as no olefinic chains exist in this vibrational region. This observation indicates that the 30-fs laser irradiated regions on CVD samples contain only sp^2 aromatic rings and the irradiated regions are completely devoid of any sp^2 olefinic fractions.

Optical (Fig. 3a-d) and SEM (Fig. 3e-h) micrographs show 30 fs-laser induced graphitized tracks on CVD samples at varying fluence (colour-coded Raman spectra shown in Fig. 1). Optical micrographs (Fig. 3a-d) display more visually contrasting and homogeneous sp^2 areas compared to the SEM (Fig. 3e-h) images; the latter show a pronounced darker centre ablation line within the main graphitized area with a lighter background, which is corresponding to the Gaussian intensity distribution of the 30-fs source beam. Notably, the ablation within the

graphitised tracks is visible even at lowest test fluence of 2.2 J/cm^2 (Fig. 3a, 3e) using the 30 fs -light, well below the nominal CVD ablation threshold fluence (*i.e.*, above 3 J/cm^2) reported for fs pulse widths exceeding 100 fs ¹⁸ as shorter pulse duration increases the beam intensity, which reduces the ablation threshold.⁷ No cracking and/or thermal damage was observed inside the sp^2 graphitised areas even at the highest test fluence (*i.e.*, 6.8 J/cm^2).

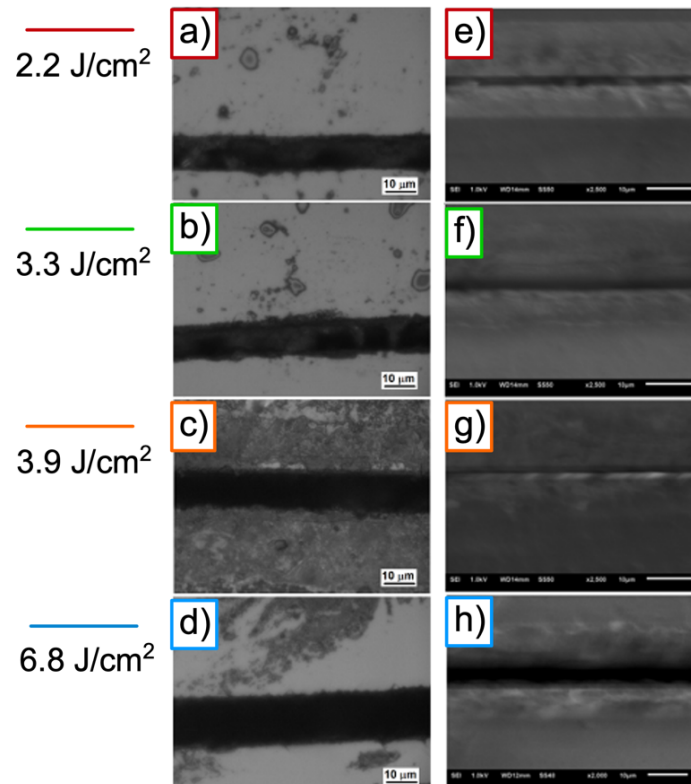


Fig. 3. Optical (a-d) and SEM (e-h) micrographs of 30 fs -irradiated regions on CVD samples at varying fluence (colour-coded to Raman spectra shown in Fig. 1); scale bar $10 \mu\text{m}$.

The width, w , of the graphitised tracks was estimated from the optical images (Fig. 3(a-d)) in order to roughly determine the sp^2 volume formation of the 30 fs -pulse irradiation process. The approximate track depth, d values were estimated from 514 nm Raman spectra by accounting for the reduced 1332 cm^{-1} sp^3 diamond core mode as suggested in the recent work by Komlenok

*et. al.*³⁰ by applying the Beer-Lambert law, which relates the attenuation of light passing through a material to the properties of the material, as expressed in Eq. (2)

$$I(d) = I_0 e^{-\alpha d} \quad (2)$$

where, for diamond, I is the 1332 cm^{-1} diamond core mode intensity, α is the diamond optical absorption coefficient, and d is depth of the sp^2 graphitized layer. The sp^2 layer absorbs both the probe beam and the scattering light and, therefore the intensity of the 1332 cm^{-1} Raman line decreases owing to the reduced probe laser and the scattered signal intensities. Consequently, the d value used to estimate the depth of the sp^2 graphitized layer, can be expressed as following:

$$d = \frac{\ln\left(\frac{I_{sp^2}^{1332}}{I_{diamond}^{1332}}\right)}{2\alpha} \quad (3)$$

where, $I_{sp^2}^{1332}$ and $I_{diamond}^{1332}$, are the intensities of 1332 cm^{-1} core diamond Raman line taken from the graphitised sp^2 regions and the original (unmodified) diamond's surface, respectively. The α has been measured empirically and reported to be $1.16 \times 10^5 \text{ cm}^{-1}$ for the laser induced sp^2 graphitized layer on diamond.³⁰

The experimentally measured widths, w and the calculated depths, d , of 30 *fs*-laser induced graphitized tracks on CVD at varying fluence are shown in Fig. 4a. The w values were found to almost linearly increase with the increasing fluence in agreement with the earlier works on *fs*-laser irradiation of diamond³⁷, diamond-like carbon³⁸, dielectrics³⁹⁻⁴⁰ and metals⁴¹. However, the estimated depth of the sp^2 tracks was found to be affected more markedly by the increase of the laser fluence, - such as the increase of fluence by approximately three ($\times 3$) times resulted in an increased depths of the graphitized tracks over an order of magnitude ($\times 10$) and, in an

instance when the irradiation was performed near or at the ablation threshold, - a fractional increase of fluence ($\sim 20\%$) resulted in a three-fold increased depth within the sp^2 graphitised areas.

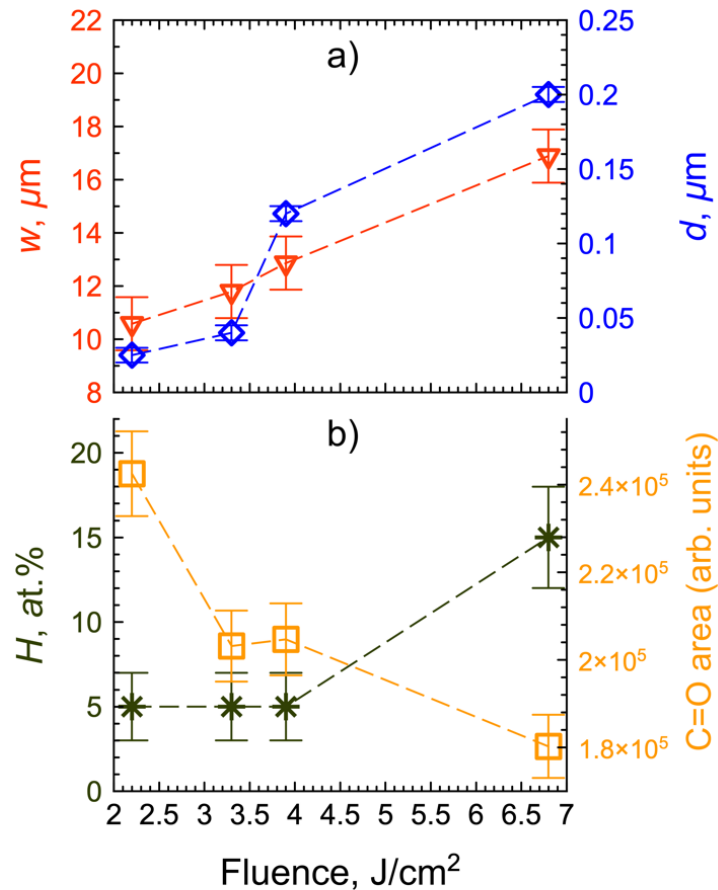


Fig. 4. a) As measured the effective widths, w , and the calculated depths, d , and b) the estimated hydrogen content, H , at.% and relative C=O contributions of 30 fs-laser induced graphitized tracks on CVD at varying laser fluence.

Notably, the d values increased from a few tens of nanometres for a low fluence (*i.e.*, *ca.* 0.025 μm for the 2.2 J/cm^2) to a sub-micron scale at a high fluence (*i.e.*, 0.2 μm for 6.8 J/cm^2). At the highest fluence of 6.8 J/cm^2 , no 1332 cm^{-1} Raman line was detectable on fs-laser induced

graphitised areas of the CVD samples. Such a non-linear effect of increasing fluence on the graphitization depths, we believe, is attributed to the non-linear optical absorption phenomena and multi-photon ionisation, which is a characteristic feature of the ultrashort *fs*-laser irradiation by which an excitation of electrons from the valence band into its conduction band is followed by a transient rapid change of the interatomic potential.²⁰ In the instance of our experiments, the ablation maxima are confined to the centre of the *sp*² graphitized tracks owing to the Gaussian intensity distribution of the beam that is consistent with the earlier findings by Abdelmalek *et al.*⁴².

Owing to a pronounced PL background displayed in all Raman spectra (see Fig. 1) an approximate hydrogen (H-) content (at. %) in the irradiated *sp*² regions could be estimated using the work of Casiraghi *et al.*²⁶ for green light excitation. It was estimated (Fig. 4b) that the *fs* laser-induced graphitised *sp*² regions generally displayed a 5 at.% protonation at or below 3.9 J/cm² fluence and a *ca.* 15 at.% for a higher 6.8 J/cm² fluence. Protonation in *fs*-laser irradiated regions is generally an indication of optical breakdown and the reduction of both the optical and Tauc gaps.^{43,44} Naturally, a suppression and cleaving of C=O carbonyl group is observed with an increasing fluence in the irradiated *sp*² regions (Fig. 1a and Fig. 4b). Increasing shielding effects are expressed by a surface-localised plasma at CVD sample irradiation site as irradiation fluence is increased resulting in plasma reflecting and/or absorbing incoming *fs*-laser light photons⁴⁵⁻⁴⁶, thus causing an extended shielding effect in the focal volume preventing an O₂ (from air) to reach the irradiation site. It is not known, however, how the degree of hydrogenation and the abundance of C=O group is distributed vertically, transversely and medially across the *sp*² photo- transformed regions in diamond. It is reasonable to assume that only the uppermost surface layer of a few nanometres thick is affected. It is, however, important to remember that in instances when the diamond *sp*³ 1332 cm⁻¹ peak is detectable for visible excitations, the actual cross-sectional area for graphite at 514 nm is *ca.* 50 larger than that of

sp^3 diamond phase as discovered by Wada *et al.*⁴⁷, and the hydrogenated amorphous carbon displays over a ~200 times larger cross-sectional area than diamond as noted by Salis and co-workers⁴⁸. These observations suggest that the estimated depth of the 30 *fs*-light photo-induced sp^2 tracks on CVD is likely to be underestimated and the actual sp^2 -rich affected regions are much larger. The current findings however, offer a valuable insight into the unique processes occurring on CVD under 50 *fs* laser light irradiation.

The following conclusions arise from our study:

- The application of an ultra-fast 30 *fs* laser irradiation to CVD samples up to a 3.9 J/cm² fluence was found to convert diamond's tetrahedral sp^3 phase into the sp^2 aromatic phase with a high degree of crystallinity without the formation of a HAZ or thermal cracking; above 3.9 J/cm² the size of planar crystalline domains in *fs* photo-irradiated regions is significantly reduced whereas the sp^2 aromatic clustering is preserved.
- *Fs*-irradiation of CVD near or at the ablation threshold was found to significantly influence the generated relative volume of the converted sp^2 phase, such as the increase of fluence by approximately three ($\times 3$) times resulted in an increased depths of the graphitized tracks over an order of magnitude ($\times 10$), and in an instance when the irradiation was performed near or at the ablation threshold, - a fractional increase of fluence (~20%, from 3.3 J/cm² to 3.9 J/cm²) resulted in a three-fold increased depth of the sp^2 graphitised areas;
- Our results indicate that the application of CVD using sub-50 *fs* pulses (i.e., 30 *fs*) is associated with a significantly reduced (by approximately 20 – 30%) CVD ablation threshold values comparing to the instances where long(er) *fs*-pulse widths (i.e., 60 – 100 *fs*) are used;
- Increased (presumably, surface-bound) hydrogenation was observed within the sp^2 graphitised regions on CVD in instances where the *fs*-irradiation was performed above

the CVD ablation threshold; no marked hydrogenation increase has been observed for 30 fs-ablation below or near the CVD ablation threshold. The C=O cleavage occurred gradually with the increasing of irradiation fluence of 30 fs laser light.

CONFLICT OF INTEREST

The authors have no conflict of interest to disclose.

AUTHOR'S CONTRIBUTIONS

BA conducted experiments, collected and analysed data and drafted the manuscript. HX, DC designed and built the experimental set up. RS revised the manuscript. IVL designed the study and revised the manuscript. MR designed the study, analysed data, drafted and critically revised the manuscript. All authors read, commented on the manuscript, gave the final approval for publication and agree to be held accountable for the work performed herein.

REFERENCES

1. Girolami, M., et al., Graphite Distributed Electrodes for Diamond-Based Photon-Enhanced Thermionic Emission Solar Cells. *Carbon* **2017**, *111*, 48-53.
2. Talamonti, C.; Kanxheri, K.; Pallotta, S.; Servoli, L., Diamond Detectors for Radiotherapy X-Ray Small Beam Dosimetry. *Frontiers in Physics* **2021**, *9*.

3. Bloomer, C.; Newton, M. E.; Rehm, G.; Salter, P. S., A Single-Crystal Diamond X-Ray Pixel Detector with Embedded Graphitic Electrodes. *Journal of Synchrotron Radiation* **2020**, *27*, 599-607.
4. Komlenok, M. S.; Dezhkina, M. A.; Sedov, V. S.; Klimenko, O. A.; Dyakov, S. A.; Gippius, N. A., Laser Ablated Nanocrystalline Diamond Membrane for Infrared Applications. *Sensors* **2022**, *22*, 829.
5. Ueda, K.; Aichi, S.; Asano, H., Direct Formation of Graphene Layers on Diamond by High-Temperature Annealing with a Cu Catalyst. *Diamond and Related Materials* **2016**, *63*, 148-152.
6. Tulić, S., et al., Covalent Diamond–Graphite Bonding: Mechanism of Catalytic Transformation. *ACS Nano* **2019**, *13*, 4621-4630.
7. Ali, B.; Litvinyuk, I. V.; Rybachuk, M., Femtosecond Laser Micromachining of Diamond: Current Research Status, Applications and Challenges. *Carbon* **2021**, *179*, 209-226.
8. Nuernberger, P.; Wolpert, D.; Weiss, H.; Gerber, G., Femtosecond Quantum Control of Molecular Bond Formation. *Proc Natl Acad Sci U S A* **2010**, *107*, 10366-70.
9. Hu, A.; Rybachuk, M.; Lu, Q. B.; Duley, W. W., Direct Synthesis of Sp²-Bonded Carbon Chains on Graphite Surface by Femtosecond Laser Irradiation. *Applied Physics Letters* **2007**, *91*, 131906.
10. Royon, A.; Petit, Y.; Papon, G.; Richardson, M.; Canioni, L., Femtosecond Laser Induced Photochemistry in Materials Tailored with Photosensitive Agents [Invited]. *Opt. Mater. Express* **2011**, *1*, 866-882.

11. Henley, S. J.; Carey, J. D.; Silva, S. R. P.; Fuge, G. M.; Ashfold, M. N. R.; Anglos, D., Dynamics of Confined Plumes During Short and Ultrashort Pulsed Laser Ablation of Graphite. *Physical Review B* **2005**, *72*, 205413.
12. Shirk, M. D.; Molian, P. A., Ultra-Short Pulsed Laser Ablation of Highly Oriented Pyrolytic Graphite. *Carbon* **2001**, *39*, 1183-1193.
13. Sainadh, U. S., et al., Attosecond Angular Streaking and Tunnelling Time in Atomic Hydrogen. *Nature* **2019**, *568*, 75-77.
14. Xing, Y.; Liu, L.; Hao, X.; Wu, Z.; Huang, P.; Wang, X., Micro-Channels Machining on Polycrystalline Diamond by Nanosecond Laser. *Optics & Laser Technology* **2018**, *108*, 333-345.
15. Haverkamp, J.; Mayo, R. M.; Bourham, M. A.; Narayan, J.; Jin, C.; Duscher, G., Plasma Plume Characteristics and Properties of Pulsed Laser Deposited Diamond-Like Carbon Films. *J. Appl. Phys.* **2003**, *93*, 3627-3634.
16. Kononenko, T. V.; Meier, M.; Komlenok, M. S.; Pimenov, S. M.; Romano, V.; Pashinin, V. P.; Konov, V. I., Microstructuring of Diamond Bulk by Ir Femtosecond Laser Pulses. *Applied Physics A* **2008**, *90*, 645-651.
17. Kononenko, V. V.; Khomich, A. A.; Khomich, A. V.; Khmel'nitskii, R. A.; Gololobov, V. M.; Komlenok, M. S.; Orekhov, A. S.; Orekhov, A. S.; Konov, V. I., Highly Oriented Graphite Produced by Femtosecond Laser on Diamond. *Applied Physics Letters* **2019**, *114*, 251903.
18. Trucchi, D. M.; Bellucci, A.; Girolami, M.; Mastellone, M.; Orlando, S., Surface Texturing of Cvd Diamond Assisted by Ultrashort Laser Pulses. *Coatings* **2017**, *7*, 1-18.

19. Wang, C. Z.; Ho, K. M.; Shirk, M. D.; Molian, P. A., Laser-Induced Graphitization on a Diamond (111) Surface. *Physical Review Letters* **2000**, *85*, 4092-4095.
20. Medvedev, N.; Jeschke, H. O.; Ziaja, B., Nonthermal Graphitization of Diamond Induced by a Femtosecond X-Ray Laser Pulse. *Physical Review B* **2013**, *88*, 224304.
21. Benner, D. C.; Rinsland, C. P.; Devi, V. M.; Smith, M. A. H.; Atkins, D., A Multispectrum Nonlinear Least-Squares Fitting Technique. *Journal of Quantitative Spectroscopy & Radiative Transfer* **1995**, *53*, 705-721.
22. Irmer, G.; Dorner-Reisel, A., Micro-Raman Studies on DLC Coatings. *Advanced Engineering Materials* **2005**, *7*, 694-705.
23. Rybachuk, M.; Hertwig, A.; Weise, M.; Sahre, M.; Mann, M.; Beck, U.; Bell, J. M., Near Infrared Optical Materials from Polymeric Amorphous Carbon Synthesized by Collisional Plasma Process. *Applied Physics Letters* **2010**, *96*, 211909.
24. Rybachuk, M.; Bell, J. M., Electronic States of Trans-Polyacetylene, Poly(P-Phenylene Vinylene) and Sp-Hybridised Carbon Species in Amorphous Hydrogenated Carbon Probed by Resonant Raman Scattering. *Carbon* **2009**, *47*, 2481-2490.
25. Ferrari, A. C., Raman Spectroscopy of Graphene and Graphite: Disorder, Electron-Phonon Coupling, Doping and Nonadiabatic Effects. *Solid State Communications* **2007**, *143*, 47-57.
26. Casiraghi, C.; Ferrari, A. C.; Robertson, J., Raman Spectroscopy of Hydrogenated Amorphous Carbons. *Physical Review B* **2005**, *72*, 085401.

27. Tuinstra, F.; Koenig, J. L., Raman Spectrum of Graphite. *The Journal of Chemical Physics* **1970**, *53*, 1126-1130.
28. Nemanich, R. J.; Solin, S. A., First- and Second-Order Raman Scattering from Finite-Size Crystals of Graphite. *Physical Review B* **1979**, *20*, 392-401.
29. Pimenta, M. A.; Dresselhaus, G.; Dresselhaus, M. S.; Cançado, L. G.; Jorio, A.; Saito, R., Studying Disorder in Graphite-Based Systems by Raman Spectroscopy. *Physical Chemistry Chemical Physics* **2007**, *9*, 1276-1290.
30. Komlenok, M. S.; Dezhkina, M. A.; Khomich, A. A.; Orekhov, A. S.; Orekhov, A. S.; Konov, V. I., Measuring the Local Thickness of Laser-Induced Graphitized Layer on Diamond Surface by Raman Spectroscopy. *physica status solidi (b)* **2019**, *256*, 1800686.
31. Cançado, L. G.; Takai, K.; Enoki, T.; Endo, M.; Kim, Y. A.; Mizusaki, H.; Jorio, A.; Coelho, L. N.; Magalhães-Paniago, R.; Pimenta, M. A., General Equation for the Determination of the Crystallite Size L_a of Nanographite by Raman Spectroscopy. *Applied Physics Letters* **2006**, *88*, 163106.
32. Girolami, M.; Bellucci, A.; Calvani, P.; Orlando, S.; Valentini, V.; Trucchi, D. M., Raman Investigation of Femtosecond Laser-Induced Graphitic Columns in Single-Crystal Diamond. *Applied Physics A* **2014**, *117*, 143-147.
33. Hu, A.; Lu, Q.-B.; Duley, W. W.; Rybachuk, M., Spectroscopic Characterization of Carbon Chains in Nanostructured Tetrahedral Carbon Films Synthesized by Femtosecond Pulsed Laser Deposition. *The Journal of Chemical Physics* **2007**, *126*, 154705.

34. Rybachuk, M.; Bell, J. M., The Observation of Sp² Fraction Disorder Using Dual Wavelength Raman Spectroscopy in a-C:H Films Fabricated Using an Open Inductively Coupled Plasma Reactor. *Diamond and Related Materials* **2006**, *15*, 977-981.
35. Jerng, S. K.; Yu, D. S.; Kim, Y. S.; Ryou, J.; Hong, S.; Kim, C.; Yoon, S.; Efetov, D. K.; Kim, P.; Chun, S. H., Nanocrystalline Graphite Growth on Sapphire by Carbon Molecular Beam Epitaxy. *The Journal of Physical Chemistry C* **2011**, *115*, 4491-4494.
36. Ferrari, A. C., Raman Spectroscopy of Graphene and Graphite: Disorder, Electron–Phonon Coupling, Doping and Nonadiabatic Effects. *Solid State Communications* **2007**, *143*, 47-57.
37. Shirk, M. D.; Molian, P. A.; Malshe, A. P., Ultrashort Pulsed Laser Ablation of Diamond. *Journal of Laser Applications* **1998**, *10*, 64-70.
38. Dumitru, G.; Romano, V.; Weber, H. P.; Pimenov, S.; Kononenko, T.; Sentis, M.; Hermann, J.; Bruneau, S., Femtosecond Laser Ablation of Diamond-Like Carbon Films. *Applied Surface Science* **2004**, *222*, 226-233.
39. Mirza, I.; Bulgakova, N. M.; Tomáščík, J.; Michálek, V.; Haderka, O.; Fekete, L.; Mocek, T., Ultrashort Pulse Laser Ablation of Dielectrics: Thresholds, Mechanisms, Role of Breakdown. *Scientific Reports* **2016**, *6*, 39133.
40. Martin, S.; Hertwig, A.; Lenzner, M.; Krüger, J.; Kautek, W., Spot-Size Dependence of the Ablation Threshold in Dielectrics for Femtosecond Laser Pulses. *Applied Physics A* **2003**, *77*, 883-884.
41. Krüger, J.; Dufft, D.; Koter, R.; Hertwig, A., Femtosecond Laser-Induced Damage of Gold Films. *Applied Surface Science* **2007**, *253*, 7815-7819.

42. Abdelmalek, A.; Sotillo, B.; Bedrane, Z.; Bharadwaj, V.; Pietralunga, S.; Ramponi, R.; Amara, E.-H.; Eaton, S. M., Origin of Femtosecond Laser Induced Periodic Nanostructure on Diamond. *AIP Advances* **2017**, *7*, 105105.
43. Tauc, J.; Grigorovici, R.; Vancu, A., Optical Properties and Electronic Structure of Amorphous Germanium. *physica status solidi (b)* **1966**, *15*, 627-637.
44. Adamopoulos, G.; Robertson, J.; Morrison, N. A.; Godet, C., Hydrogen Content Estimation of Hydrogenated Amorphous Carbon by Visible Raman Spectroscopy. *J. Appl. Phys.* **2004**, *96*, 6348-6352.
45. Zinovik, I.; Povitsky, A., Dynamics of Multiple Plumes in Laser Ablation: Modeling of the Shielding Effect. *Journal of Applied Physics* **2006**, *100*, 024911.
46. SallÈ, B.; Gobert, O.; Meynadier, P.; Perdrix, M.; Petite, G.; Semerok, A. F., Femtosecond and Picosecond Laser Microablation: Ablation Efficiency and Laser Microplasma Expansion. *Applied Physics A* **1999**, *69*, S381-S383.
47. Wada, N.; Gaczi, P. J.; Solin, S. A., "Diamond-Like" 3-Fold Coordinated Amorphous Carbon. *Journal of Non-Crystalline Solids* **1980**, *35-36*, 543-548.
48. Sails, S. R.; Gardiner, D. J.; Bowden, M.; Savage, J.; Rodway, D., Monitoring the Quality of Diamond Films Using Raman Spectra Excited at 514.5 Nm and 633 Nm. *Diamond and Related Materials* **1996**, *5*, 589-591.